Earth and Planetary Science Letters 285 (2009) 297–308

Contents lists available at ScienceDirect

Earth and Planetary Science Letters

journal homepage: www.elsevier.com/locate/epsl

Caloris impact basin: Exterior geomorphology, stratigraphy, morphometry, radial sculpture, and smooth plains deposits

Caleb I. Fassett [a,*], James W. Head [a], David T. Blewett [b], Clark R. Chapman [c], James L. Dickson [a], Scott L. Murchie [b], Sean C. Solomon [d], Thomas R. Watters [e]

[a] Department of Geological Sciences, Brown University, 324 Brook Street, Box 1846, Providence, RI 02912, USA
[b] Johns Hopkins University Applied Physics Laboratory, 11100 Johns Hopkins Road, Laurel, MD 20723, USA
[c] Southwest Research Institute, 1050 Walnut St. (Suite 300), Boulder, CO 80302, USA
[d] Department of Terrestrial Magnetism, Carnegie Institution of Washington, 5241 Broad Branch Road, NW, Washington, DC 20015, USA
[e] Center for Earth and Planetary Studies, National Air and Space Museum, Smithsonian Institution, Washington, DC 20013, USA

ARTICLE INFO

Article history:
Accepted 15 May 2009
Available online 24 June 2009

Keywords:
Mercury
MESSENGER
Caloris basin
stratigraphy
smooth plains

ABSTRACT

The Mariner 10 flybys revealed the eastern third of the Caloris basin and demonstrated its importance as a chronostratigraphic marker for the geological history of Mercury. Uncertain after that mission were the size of the basin, the full distribution of materials deposited or modified during the impact process, and the stratigraphic and age relationships between Caloris and surrounding terrain. Images obtained during MESSENGER's January 2008 flyby of Mercury revealed that the Caloris basin is ~15% larger than previously estimated and moderately elliptical (~1525 by ~1315 km). Basin-related sculpture and secondary craters are dispersed widely in areas surrounding the basin, confirming the widespread significance of this event as a stratigraphic marker. Units mapped around Caloris on the basis of Mariner 10 data are generally recognized in regions observed for the first time by MESSENGER, including most facies of the Caloris Group (the Caloris Montes, Odin Formation, and Van Eyck Formation). The only unit without obvious exposures in MESSENGER images is the Nervo Formation, which was originally interpreted as impact melt or fallback ejecta. New measurements of the size-frequency distribution of impact craters both within the Caloris basin and on surrounding units, particularly the Odin Formation, support the hypothesis that the vast majority of circum-Caloris plains postdate the basin and are likely volcanic. The MESSENGER observations re-emphasize the importance of understanding the exterior stratigraphy of the basin in order to utilize the Caloris event as a discrete time horizon in the geological history of Mercury.

1. Introduction and background

The Caloris impact basin is the most prominent large multi-ring basin yet observed on Mercury. As such, it has been the subject of intense study since the three flybys of Mercury by Mariner 10, which provided a detailed view of the eastern third of the basin (Murray et al., 1974; McCauley, 1977; McCauley et al., 1981). During the first flyby of Mercury by the MErcury Surface, Space ENvironment, GEochemistry, and Ranging (MESSENGER) spacecraft (Solomon et al., 2008), the Mercury Dual Imaging System (MDIS) (Hawkins et al., 2007) acquired the first images of the basin in its entirety. The first flyby also provided excellent image coverage of the Caloris surroundings, as ~95% of the region within one basin diameter was imaged following the first flyby, compared with the ~40% of this region observed by Mariner 10. New observations of the basin interior itself have been described by Murchie et al. (2008) and Watters et al. (2009-this issue).

In this paper, we use the new imaging coverage of the region around Caloris afforded by MESSENGER to address three primary questions: (1) What are the characteristics and extent of geological materials associated with Caloris? (2) What is the morphometry of the Caloris basin, and what might this tell us about the impact event? (3) What are the stratigraphic and age relationships between Caloris and its surrounding plains units?

The modification of the region around large impact basins such as Caloris is apparent on all solid bodies with ancient surfaces, with the Moon providing some of the best-understood examples (see Spudis, 1993). Around Imbrium basin, radially textured sculpture was recognized during pioneering telescopic studies of the Moon (Gilbert, 1893). This radial sculpture is likely a result of the erosion and reworking of pre-existing material as ejecta from the basin impacted the surface surrounding the basin (Baldwin, 1963). The scale of these features clearly demonstrates the large role that impact basins play in modifying and redistributing material across a planetary surface (e.g., McGetchin et al., 1973; Haskin, 1998; Haskin et al., 1998; Petro and Pieters, 2005, 2006). In this paper, we describe new evidence for the nature of similar geological processes on Mercury, particularly as was

* Corresponding author.
E-mail address: Caleb_Fassett@brown.edu (C.I. Fassett).

0012-821X/$ – see front matter © 2009 Elsevier B.V. All rights reserved.
doi:10.1016/j.epsl.2009.05.022

recorded in sculpture around the Caloris basin, as well as other geological units associated with the basin.

From Mariner 10 mapping and stratigraphic analysis, McCauley et al. (1981) described discrete geological units related to the basin, which they defined as the Caloris Group. The identification of these units and the association with the Caloris-forming event were intended to establish a stratigraphic marker that could be applied across a large area of the planet, similar to the use of basin materials as stratigraphic markers on the Moon (Shoemaker and Hackman, 1962; McCauley et al., 1981; Spudis and Guest, 1988). The mapped extent (Schaber and McCauley, 1980; Guest and Greeley, 1983) for the Caloris Group facies defined from Mariner 10 images is shown in Fig. 1, along

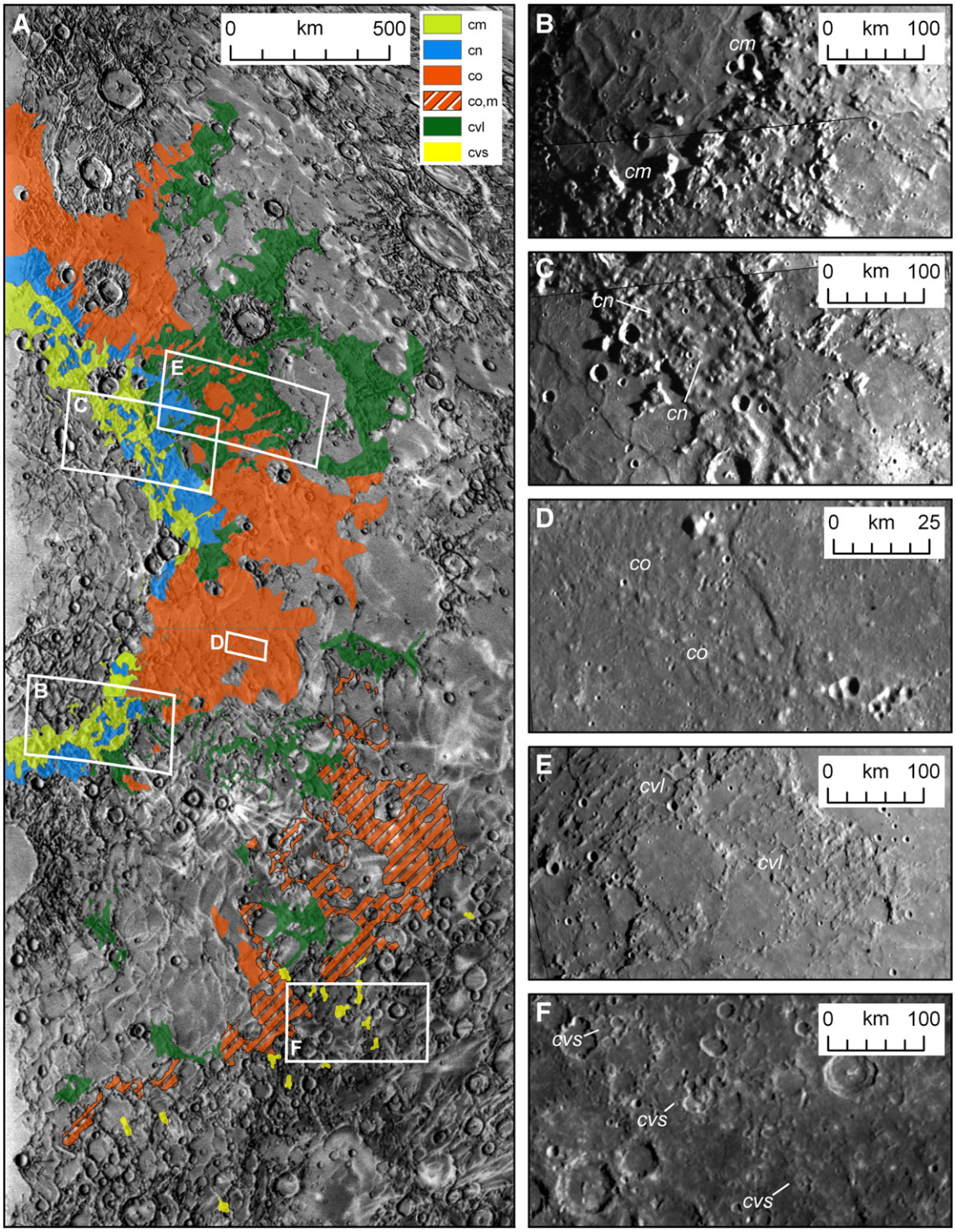

Fig. 1. (A) Mapping of the Caloris Group in the H-3 and H-8 quadrangles by Guest and Greeley (1983) and Schaber and McCauley (1980), respectively. (B–F) Type examples of the Caloris Group materials seen in Mariner 10 images, after McCauley et al. (1981): (B) The Caloris Montes Formation (*cm*) is defined by the blocky material surrounding the central basin along the presumed main rim. (C) The Nervo Formation (*cn*) consists of intermontane plains in the immediate Caloris surroundings that locally appear draped on *cm*. (D) The Odin Formation (*co*) consists of the hummocky plains material in the Caloris surroundings and is characterized by kilometer-scale blocks. Where Schaber and McCauley (1980) interpreted the Odin Formation as mantling older terrain, they mapped it as *co,m*. (E) The Van Eyck Formation, lineated facies (*cvl*), is characterized by lineated material with grooves and ridges extending radially from Caloris. (F) The Van Eyck Formation, secondary crater facies (*cvs*), consists of mapped Caloris secondary clusters and chains.

with type areas illustrating their surface morphology. On the basis of Mariner 10 images, these facies have characteristics as follows:

(1) The Caloris Montes (*cm*; Fig. 1B) define the topographic rim around the basin and are comprised of numerous discrete uplifted blocks tens to hundreds of kilometers across. In some locations, these blocks form nearly continuous ranges, while in other sections blocks are discontinuous and expressed as discrete knobs, similar to the main rim of Imbrium and the Montes Rook at Orientale (Head, 1974a). Individual sections also vary substantially in size, height, and the degree to which they appear embayed by Caloris interior and exterior plains material.

(2) The Nervo Formation (*cn*, Fig. 1C) consists of smooth plains draped within the Caloris Montes massifs, perhaps formed as fallback ejecta (McCauley et al., 1981) or impact melt (Spudis and Guest, 1988). The Nervo Formation was most extensively

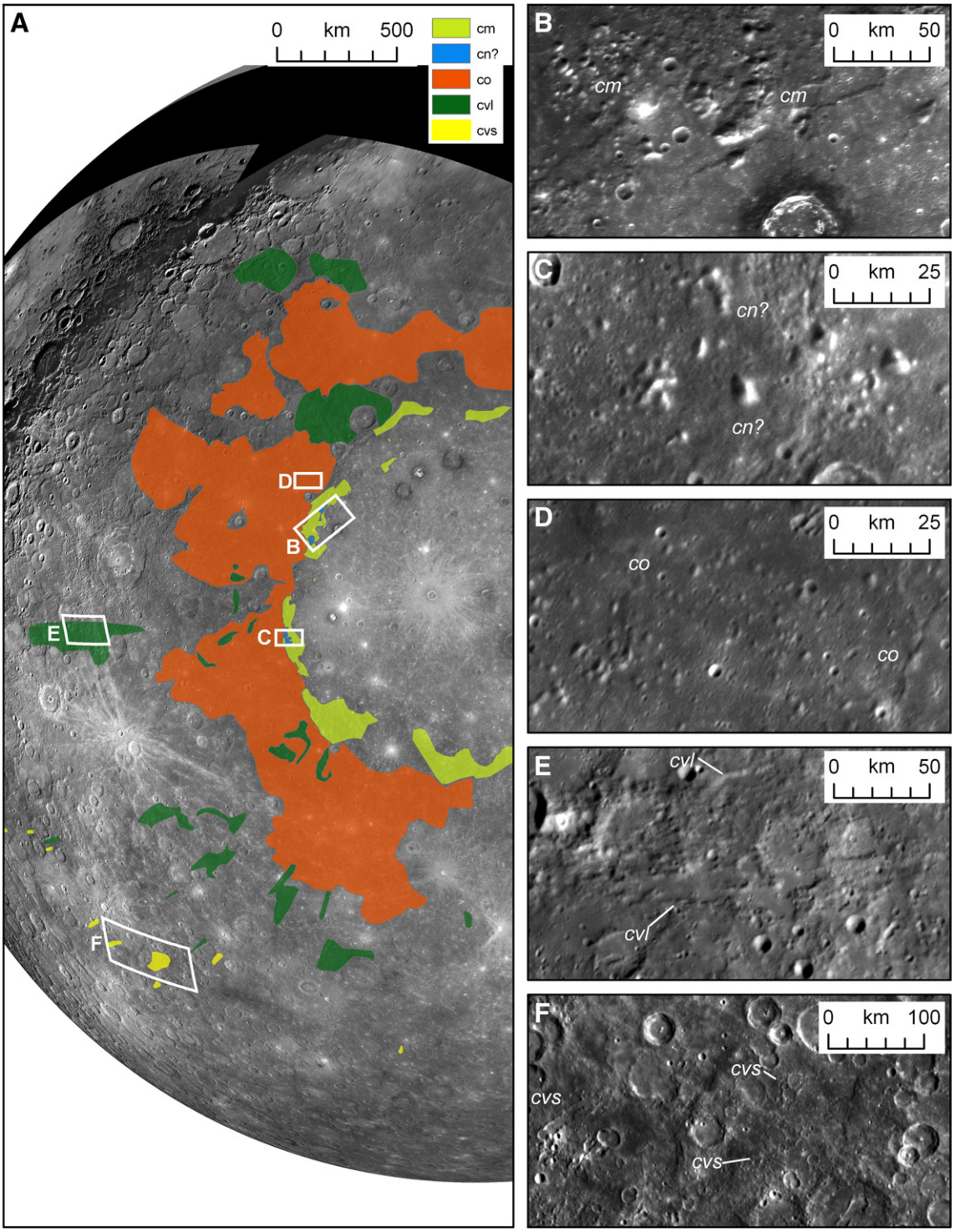

Fig. 2. (A) Map of the distribution of Caloris Group materials in MESSENGER data. (B–F) Type examples of the Caloris Group materials in MESSENGER data: (B) the Caloris Montes Formation (*cm*); (C) possible example of the Nervo Formation (*cn*); (D) the Odin Formation (*co*); (E) the Van Eyck Formation, lineated facies (*cvl*); (F) the Van Eyck Formation, secondary crater facies (*cvs*). Panels (B–D) and (F) are from MDIS narrow-angle camera (NAC) mosaic 2 (image sequence EN0108826517M–EN0108827087M); panel (E) is from the MDIS NAC departure mosaic 1 (image sequence EN0108828094M–EN0108828654M).

mapped northeast of the basin, where lobes of possible ejecta and melt were thought to be visible.

(3) The Odin Formation (*co*, Fig. 1D) is a circum-Caloris plains unit, characterized by numerous kilometer-scale hummocky hills. These knobs or hills have typically been interpreted as ejecta blocks, although their precise mode of origin is uncertain (e.g., Spudis, 1993). McCauley et al. (1981) noted that the boundaries of the Odin Formation are diffuse and that its relationship with Caloris is more ambiguous than the other group members they defined. In some regions, Odin Formation material was interpreted as mantling or draping the pre-Caloris highlands (Schaber and McCauley, 1980; *co,m* in Fig. 1A).

(4) The Van Eyck Formation is divided into two subunits, secondary craters and lineated terrain, both of which are found radial to the basin. Lineations (*cvl;* Fig. 1E) and ridges extend to substantial distances from the basin rim (thousands of kilometers), and probable clusters of basin secondaries (*cvs*; Fig. 1F) are recognizable at even greater distances. The Van Eyck Formation is directly comparable to sculpture around lunar basins such as Imbrium; we therefore use the phrase Caloris sculpture interchangeably with the Van Eyck Formation.

Finally, the plains on the Caloris basin floor were not included in the Caloris Group (McCauley et al., 1981). McCauley et al. (1981) noted that although this unit is of uncertain origin, it "clearly represents a deep-fill unit that now obscures the [original] floor of the basin." Data from MESSENGER support this assessment and suggest that the interior plains have a volcanic origin (see Murchie et al., 2008; Watters et al., 2009-this issue).

2. New observations of Caloris exterior stratigraphy

The new image coverage provided by MESSENGER allows us to extend the observations of the circum-Caloris region into areas that were not imaged by Mariner 10. These new data suggest that most of the formations originally mapped as the Caloris Group east of Caloris are recognizable west of the basin as well (Fig. 2). In this section, we describe specific observations of each facies in turn. First, however, we note that MDIS wide-angle camera (WAC) multispectral images show relatively little color variation among the various members of the Caloris Group (Murchie et al., 2008) (Fig. 3). In contrast, there is a marked difference between Caloris Group materials and the Caloris interior plains, in that the interior plains have a higher reflectance and are redder (Robinson et al., 2008; Murchie et al., 2008) (Fig. 3). Although observations from color alone are consistent with a model whereby the Caloris Group facies are directly associated with the basin itself and have an origin distinct from that of the interior plains, this hypothesis is inconsistent with other observations, most notably differences in the size-frequency distribution of impact craters on different units (see Section 4.4).

2.1. The Caloris Montes and Caloris rim

In MESSENGER images, outcrops of the Caloris Montes are apparent around most of the circumference of its rim (Fig. 2A). These massifs, as well as the extent of distinct Caloris interior fill, demonstrate that Caloris is somewhat larger in diameter than was thought on the basis of Mariner 10 images. However, the actual geometry of the basin topographic rim is complex, as is often the case with large multi-ringed basins (e.g., Spudis, 1993).

One such complexity is that, unlike what was observed in Mariner 10 data, at least several massifs of Caloris Montes-like material are located well inside the Caloris floor unit. The largest such block is 80 km × 40 km (43°N, 150°E; Fig. 4B). This massif may be a short segment of a poorly exposed section of the main rim of Caloris. Alternatively, it may be a remnant of an inner ring, similar to Mons Pico or the Montes Recti inside Imbrium. We tentatively favor the first hypothesis, for the following reasons: (1) the distance from this massif to the center of the basin is ~670 km, very similar to the distance from the inferred center of the basin to the better-defined southern rim; (2) this massif is of comparable topographic expression to other Caloris Montes blocks and appears to have greater relief than the basin plains margin to the north; and (3) the orientation and inclusion of the massif in the basin rim are consistent with a shape represented by an ellipse determined using only the more well-defined sections of the rim, including those observed in Mariner 10 images (Fig. 4A, Section 4.1).

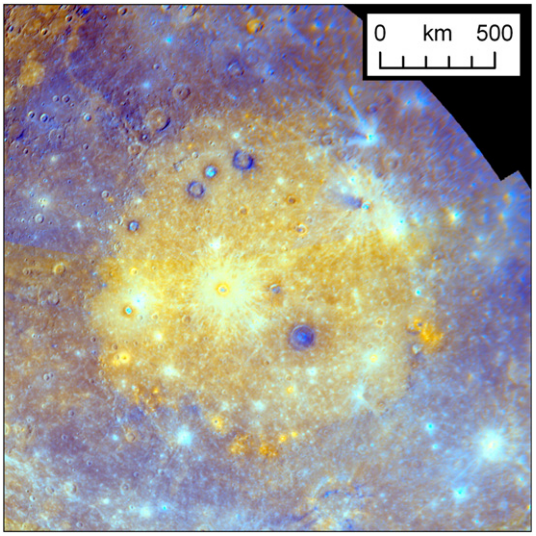

Fig. 3. Separation of major color units by means of the principal component (PC) analysis of Robinson et al. (2008), reprojected to an orthographic projection centered on Caloris (30°N, 162°E). The red channel is the inverse of the second principal component (PC2, mainly capturing color variation), the green channel is PC1 (capturing reflectance variation), and the blue channel is a ratio of the 430-nm and 560-nm visible bands. Most Caloris Group materials have similar color properties, clearly distinct from the interior plains (Robinson et al., 2008; Murchie et al., 2008).

Even in regions where the basin rim is well defined, the Caloris Montes are clearly discontinuous in MESSENGER images, as was observed in the Mariner 10 data. These gaps may reflect burial of low sections of the rim. Qualitatively, the Caloris Montes appear more completely buried by volcanic plains in their western and northern sectors than in the eastern sector observed by Mariner 10 (see Section 4.1). Other MESSENGER observations have suggested that the rim region hosted centers of volcanic activity, on the basis of color anomalies (Fig. 3) and apparent embayment relationships with low massifs in the Caloris Montes (Murchie et al., 2008; Head et al., 2009-this issue). These volcanic centers, along with other vents yet to be recognized, may have contributed to the emplacement of the Caloris interior and exterior plains, which appear responsible for embaying the Caloris Montes and Caloris rim.

2.2. The Nervo Formation

The Nervo Formation was mapped as the areas of smooth plains in the immediate basin surroundings and was interpreted as locally draped over and burying the Caloris Montes (Fig. 1B). Unambiguous exposures of the Nervo Formation are absent in MESSENGER data. In Fig. 2B, we show an example of possible Nervo Formation, guided by where we would expect it from Mariner 10 observations (within the Caloris Montes).

The lack of an unambiguous geomorphic signature of the Nervo Formation in MESSENGER data may be attributable to either observing conditions or surface geology. Three possible explanations are: (1) The Caloris Montes region may have been more deeply buried along the

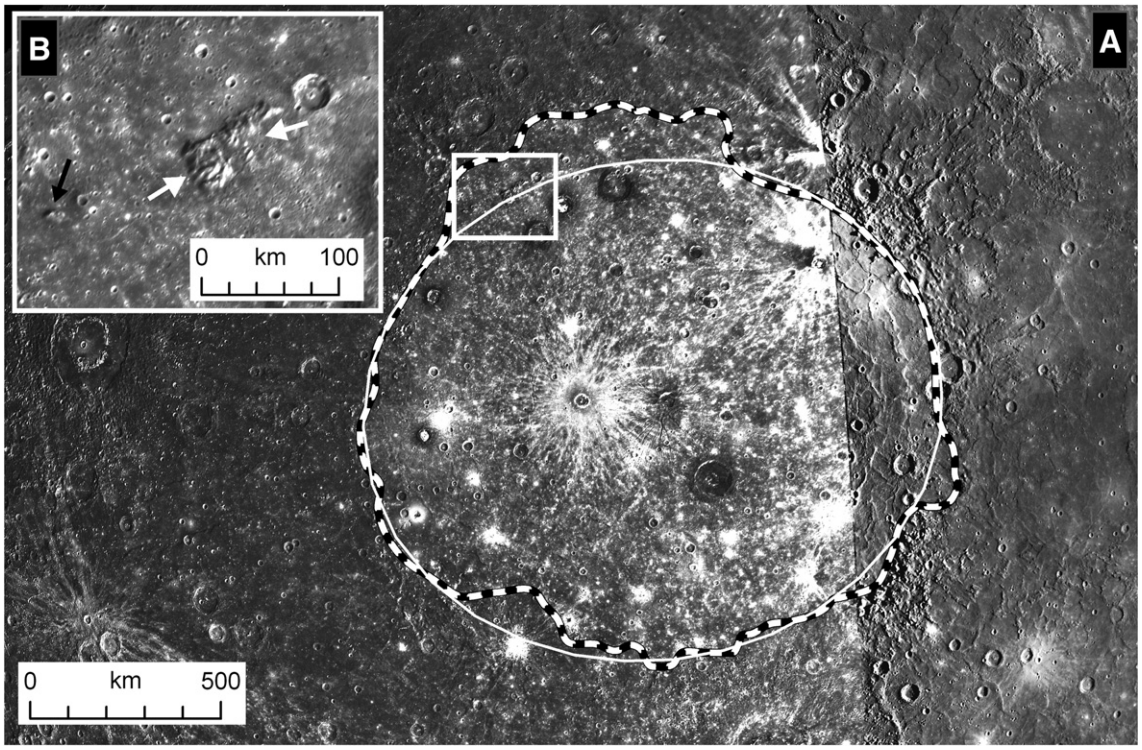

Fig. 4. (A) The extent of the Caloris interior plains (dashed line) and the shape of the Caloris basin that provides a best fit through the most prominent outcrops of the Caloris Montes massifs (white oval). The base image is a composite of MESSENGER (left) and Mariner 10 (right) image mosaics. (B) A major massif surrounded by Caloris floor material; if the best-fit ellipse is the correct representation of the original basin shape, this massif represents the only prominent exposed portion of the north rim of the basin. White arrows mark the location of the best-fit ellipse, for which the northern part of the basin was not used as a constraint. The black arrow shows a smaller massif of *cm* also surrounded by the Caloris interior plains. Mosaic of MDIS NAC images EN0108826617M, EN0108826622M, EN0108826682M, and EN0108826687M.

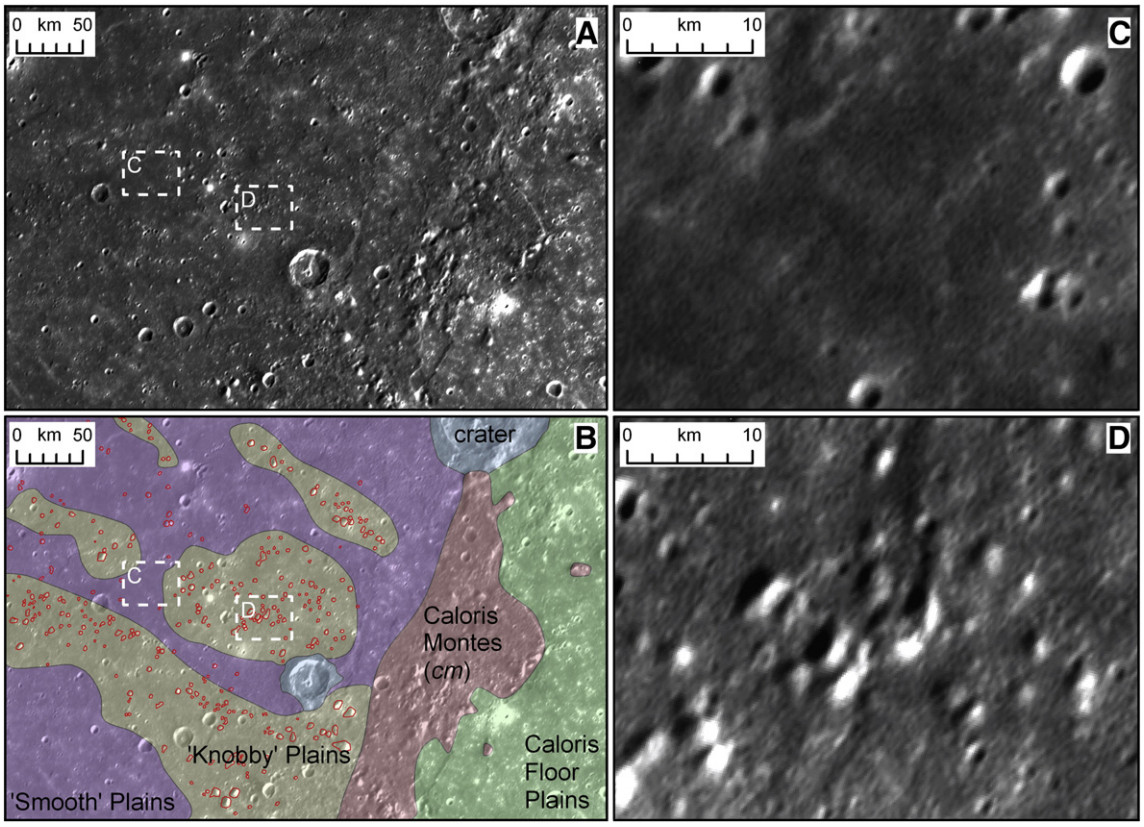

Fig. 5. The Odin Formation (*co*). (A) Region just west of Caloris basin, centered at 40°N, 140°E. Mosaic of MDIS NAC images EN0108826607M, EN0108826612M, EN0108826617M, EN0108826672M, EN0108826677M, and EN0108826682M. (B) Sketch map of principal materials in this region; knobs are outlined in red. Both the smoothest and knobbiest portions of these plains would likely have been mapped as Odin Formation from Mariner 10 images. (C) Sample texture of a smooth region of the plains (MDIS NAC image EN0108826612M). (D) Sample texture of a knobby portion of the plains (MDIS NAC image EN0108826677M). Note that (C) and (D) are only ~100 km apart. Similar variations in the density of knobs are seen throughout (A) and (B).

western rim seen by MESSENGER than the eastern rim observed by Mariner 10, limiting Nervo Formation exposure. (2) The Nervo Formation or "fallback ejecta" may not be truly exposed on *either* the eastern or western rim. Under this explanation, what has been mapped as the Nervo Formation may be geologically equivalent to an interior or exterior plains unit. (3) The Nervo Formation may be present along the western rim of Caloris, and our inability to recognize it in MESSENGER images may be a result of the illumination geometry of the first flyby. The Nervo Formation was first mapped and described on the basis of near-terminator Mariner 10 images. MESSENGER data obtained during the orbital phase of the mission will help delineate the actual extent of the Nervo Formation around the basin and establish which (if any) of these three explanations is correct.

2.3. The Odin Formation

Unlike the Nervo Formation, the Odin Formation is immediately recognizable in the circum-Caloris region in MESSENGER data (Fig. 2C). The Odin Formation is defined by the presence of kilometer-scale knobs in otherwise typical smooth plains (Fig. 5). In both MESSENGER and Mariner 10 images, the formation is commonly apparent adjacent to the Caloris rim/Caloris Montes (Figs. 1, 2), but patches of probable Odin material extend to distances of ~800 km from the Caloris rim. The density of knobs in the Odin Formation appears to decrease moderately away from the Caloris rim, supporting the hypothesis that these knobs are genetically related to the basin in some manner.

We have mapped a sample region of the Odin Formation from MESSENGER observations to help constrain the distribution and origin of the knobs (Fig. 5). The median linear dimension of the observed knobs is ~2 km. Even at nearly the same radial distance from the Caloris rim, exposed plains have substantial differences in texture, ranging from smooth and featureless (Fig. 5C) to densely covered by knobs (Fig. 5D). The cause of this variation in texture is unclear, but may reflect variations on a local scale in the thickness of volcanic resurfacing exterior to Caloris. Possible interpretations of the Odin Formation and its characteristic knobs are discussed in more detail in Sections 3 and 4.4.

2.4. Caloris secondaries and sculpture: the Van Eyck Formation

The Van Eyck Formation radial lineations and secondaries are the most prominent features in the circum-Caloris region resulting from basin formation. Van Eyck material is divided into two closely related sub-classes (McCauley et al., 1981): lineations and secondary craters. In Fig. 6, we show the extent of the Van Eyck Formation in MESSENGER data.

The typical expression of the lineated sculpture is as a series of ridges and troughs that are 5–30 km wide (Fig. 7). In some locales, especially far from the Caloris rim, trough walls can appear cuspate. Lineations occasionally transition into the connected rims of craters or crater chains that formed as secondary craters. For this reason, the two subfacies of Van Eyck Formation are not fully separable. In some regions, secondary crater chains clearly contributed to the formation of the lineations that most prominently define the Van Eyck Formation (e.g., Fig. 7E).

MESSENGER images reveal that this sculpture is distributed much more broadly (Fig. 6) than was apparent on the basis of Mariner 10

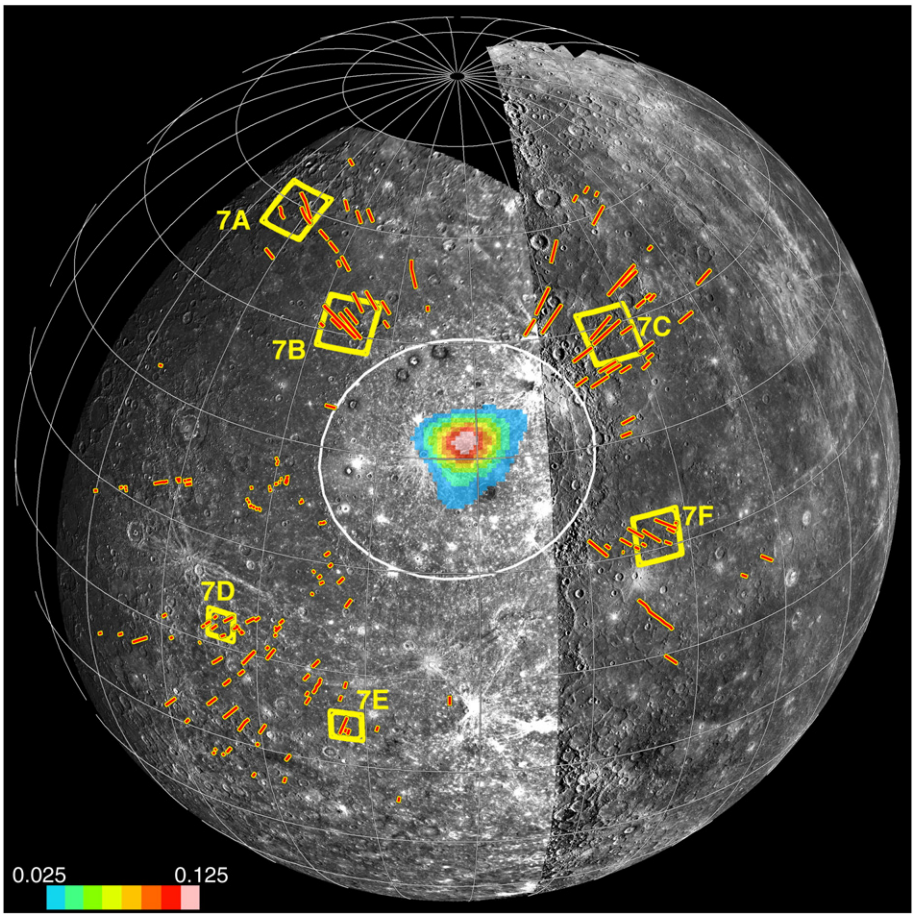

Fig. 6. Distribution map of the Van Eyck Formation lineated facies (*cvl*) or "Caloris sculpture" (orthographic projection centered at 30°N, 162°E). Locations of Fig. 7A–F are shown in yellow boxes. The color plot inside the basin is a density map of intersection points (density of intersections per square kilometer; pink is highest), derived by projecting the lineations to their source point as great circles. Base image is a composite of MESSENGER (left) and Mariner 10 (right) image mosaics.

data alone (e.g., Spudis and Guest, 1988). The mappable extent of the Van Eyck Formation will likely expand further, as regions immediately north and south of the basin are imaged under less challenging illumination conditions. More distal lineations tend to be smaller (e.g., Fig. 7D,E) than more proximal Van Eyck lineations (Fig. 7B,F), and lineations are occasionally associated with small secondary crater chains (Figs. 2E, 7D). Radial lineations are also clustered in space and appear at the same stratigraphic level. These trends are consistent with what would be expected from impact erosion. For the Moon, some have argued (e.g., Hartmann, 1963) that portions of the radial texturing related to Imbrium might be structural. We find no evidence that would support this mechanism for forming the sculpture observed around Caloris.

As on the Moon, there are often small regions of smooth plains materials in the low-lying regions in the heavily sculpted highlands (Fig. 7D,E). Possible origins for the plains immediately adjacent to the Van Eyck Formation include ballistic sedimentation of ejecta, as well as volumetrically important mass movements triggered as secondaries struck the surface around the basin (e.g., Oberbeck et al., 1975; Oberbeck, 1975). Under this interpretation, these plains may be analogous to the breccia-dominated light lunar plains, such as the Cayley Formation sampled at the Apollo 16 landing site (e.g., Head, 1974b; Spudis, 1984; Stöffler et al., 1985). Alternatively, these regions of smooth plains adjacent to the Van Eyck Formation may be small areas of volcanism in the highlands (see Section 4.4).

Initial observations suggest that Caloris secondaries are more difficult to map than the Caloris sculpture, although some probable secondary clusters from Caloris are observed (Figs. 1A,F; 2A,F). Chains and clusters of secondary craters can be difficult to link to a particular parent crater at great distance, a problem that is exacerbated on Mercury by the apparent high background density (and high production rate) of secondary craters at sizes <6–8 km diameter (Strom et al., 2008). For the Moon, the recognition of probable secondaries associated with large basins such as Imbrium required careful analysis of crater shape, downrange overlap, clustering, and radial distribution (e.g., Wilhelms, 1976b). Most Imbrium clusters are in regions downrange from the Imbrium sculpture (e.g., Fig. 15d in Head, 1975). Examples of possible Caloris secondary clusters are found in similar locations downrange of Van Eyck lineated terrain (Fig. 2E). Improved recognition and mapping of Caloris secondaries is an important subject for future analysis and will be greatly aided by the coverage, resolution, and illumination that will be provided by MESSENGER.

3. The crater populations of Caloris Group facies

One straightforward technique for estimating the ages and geological relationships among stratigraphic units is the measurement of superposed crater populations. With MESSENGER data, Strom et al. (2008) compared a broad portion of the exterior plains of Caloris (including the Odin Formation and surrounding smooth plains) with the interior plains, and they found fewer superposed craters on the exterior plains. Given that the interior plains must postdate the Caloris event and are likely volcanic (Murchie et al., 2008), this result implies that at least some of the exterior plains were emplaced well after basin formation, likely by volcanism (Strom et al., 2008). Here, we describe crater counts for specific Caloris Group facies, with the aim of understanding the relative ages of and geological relationships between the basin itself and its associated units.

We have used two separate techniques and count regions to attempt to measure a crater size-frequency distribution for the Caloris

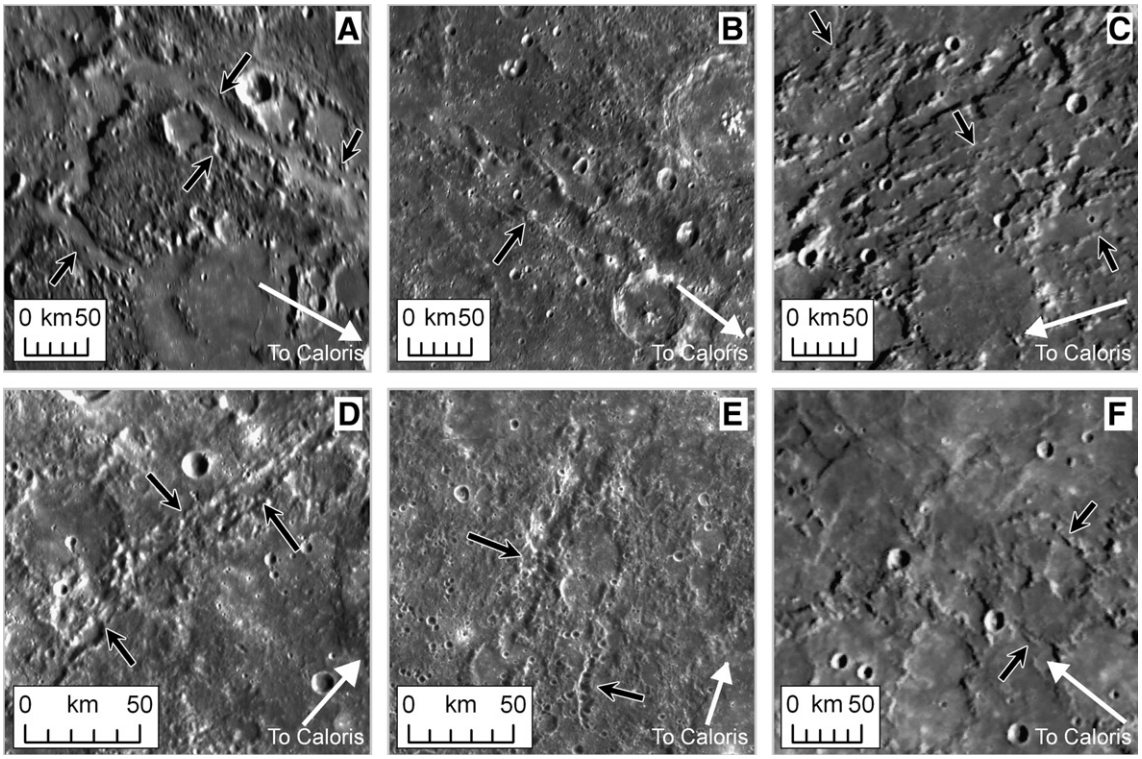

Fig. 7. Examples of the Van Eyck Formation lineations (Caloris sculpture) in MESSENGER (A–B,D–E) and Mariner 10 (C,F) data; see Fig. 6 for location context. Each subframe is in a local sinusoidal projection; black arrows highlight features; white arrow shows direction to Caloris. (A) Van Eyck Formation 1000 km northwest of the Caloris rim; in this location, the lineations are floored by smooth plains (MDIS NAC image EN0108828629M). (B) A proximal exposure of the Van Eyck Formation, along the northwestern rim of the basin (MDIS NAC images EN0108826607M, EN0108826612M, and EN0108826617M). (C) A proximal exposure along the northeastern margin of Caloris; here the Van Eyck lineations are mainly expressed as sculpted ridges with smooth plains filling low-lying regions across the entire scene (Mariner 10 image FDS-189). (D) 850 km southwest of the Caloris rim (MDIS NAC images EN0108827057M, EN0108827062M), and (E) 900 km south–southwest of the Caloris rim (MDIS NAC images EN0108825824M, EN0108825829M, EN0108825929M). In both (D) and (E), lineations commonly have cuspate boundaries suggesting that they formed by secondary impacts. Smooth plains between the lineations in these areas may result from impact processes (see Section 4.3), similar to those that formed the Cayley Formation on the Moon. (F) Southeast of the basin; here lineations are embayed and partially buried by smooth plains; however, since they remain visible, the smooth plains in this region are <500 m thick, the estimated relief of the sculpture elements (Mariner 10 image FDS-252).

basin event itself. First, we counted craters on the Caloris Montes along the Caloris rim (Fig. 8A) using both Mariner 10 and MESSENGER images, excluding regions with poor illumination geometry immediately north and south of the basin. These data imply that the Caloris Montes have a significantly higher crater density than the Caloris interior plains (Fig. 8B,C). The number of craters $N(20)$ having a diameter $D \geq 20$ km normalized to an area of 10^6 km^2 for the Caloris Montes is 54 ± 12, compared with $N(20) = 23 \pm 4$ for the interior plains. For craters having $D \geq 10$ km, we find $N(10) = 103 \pm 16$ for the Caloris Montes, and $N(10) = 75 \pm 7$ for the interior plains. (Reported confidence intervals are $\pm$one standard deviation, taken to equal the square root of the number of craters normalized to an area of 10^6 km^2). The second technique that we use to infer the age of the Caloris basin is a buffered approach to counting craters on the Van Eyck lineated terrain (Tanaka, 1982; Fassett and Head, 2008). Specifically, from the mapped lineated terrain (Fig. 6) we counted craters only within a strict buffer along traces of the Caloris sculpture, requiring that each crater counted be clearly superposed (centered within one crater radius) on a lineation. The count area relevant to a given crater size is computed independently for each crater diameter (Fassett and Head, 2008). The results of this methodology give very similar cumulative crater densities to those for the Caloris Montes, with $N(20) = 50 \pm 11$ and $N(10) = 126 \pm 20$ (Fig. 8B). Along with a similar crater density, the count on the sculpture has a similar size-frequency distribution as that for the basin rim, at least for craters between 16 and 64 km in diameter (Fig. 8C).

Both of these estimates of the crater population characteristic of the Caloris event have shapes similar to that of "Population 1" craters, which may date to the late heavy impact bombardment of the inner Solar System (Strom et al., 2005, 2008). This shape contrasts with that of the crater size-frequency distribution on both the Caloris interior and exterior plains, which is more similar to that of "Population 2" craters (Strom et al., 2005, 2008). The steeply decreasing frequency of craters at diameters smaller than 16 km in the Caloris rim count is due primarily to difficult lighting conditions, which limit crater recognition. It may also result, in part, from preferential loss of small craters in

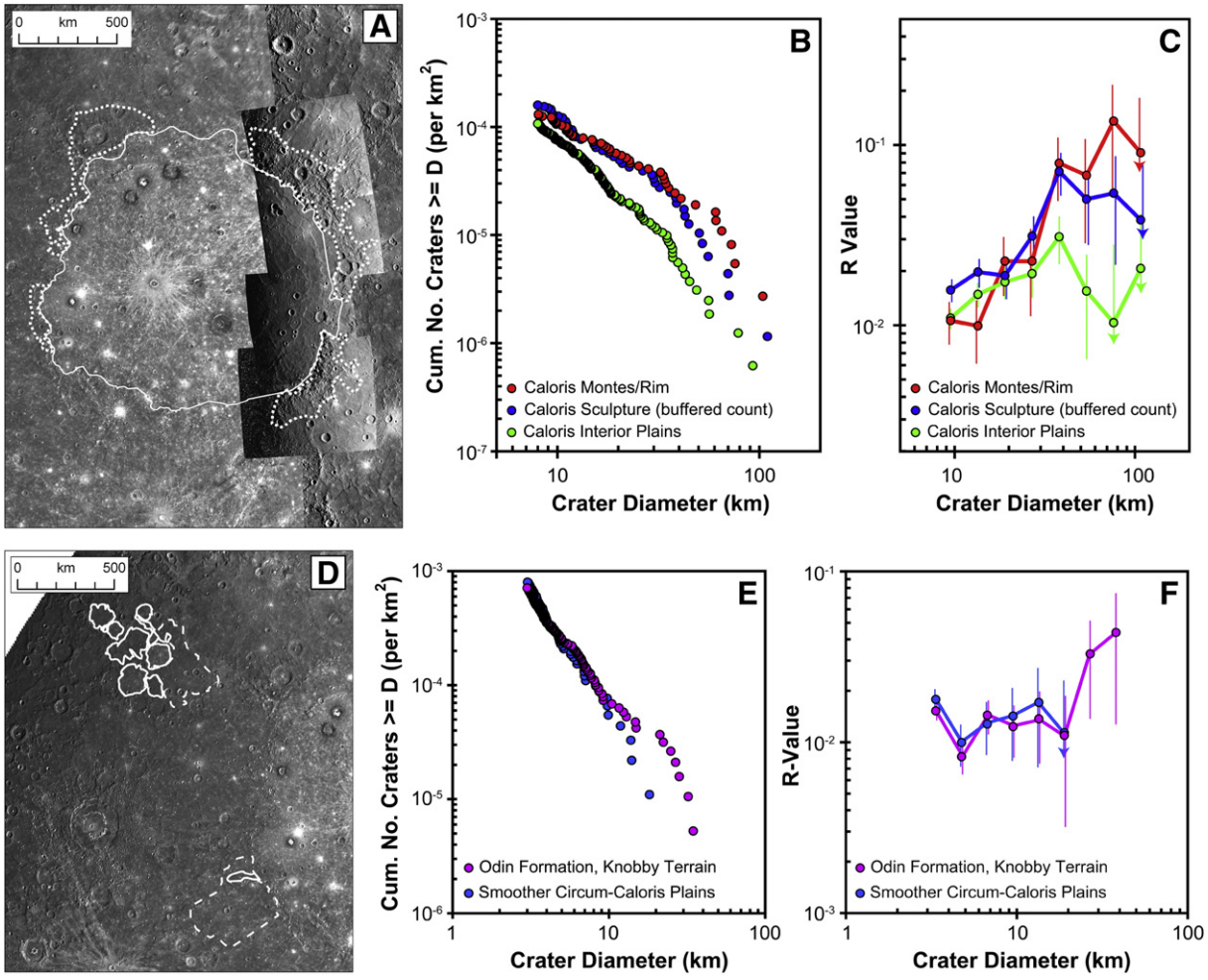

Fig. 8. (A) Regions for crater counts on the Caloris interior plains (solid) and Caloris rim (dots). Count areas were 1.6 million km^2 for the interior plains and 0.37 million km^2 for the Caloris rim. (B) Cumulative crater size-frequency plot showing the density of craters on the Caloris interior plains, Caloris Montes, and lineated Van Eyck Formation/Caloris sculpture. The lineated terrain and Caloris Montes have a similar density of craters, which we consider a reasonable representation of the size-frequency distribution characteristic of the time immediately following the Caloris event. Both have much denser populations of craters with $D \geq 20$ km than the interior (or exterior) plains. (C) R-plot of the Caloris interior plains, Caloris Montes, and lineated Van Eyck Formation (same data as part B). The Caloris Montes and Caloris sculpture have a distribution similar to that of Population 1 craters (Strom et al., 2005), and that for the interior plains (and exterior plains) is similar to that of Population 2 (see also Strom et al., 2008). Error estimates are from the square root of the number of craters in a given bin; arrows are shown for bins with a single crater. (D) Count regions for knobby (dashed) and smooth (solid) subregions of the circum-Caloris plains. Count areas were 0.19 million km^2 for the knobby terrain and 0.10 million km^2 for the smooth subregion. (E) The cumulative crater plot, and (F) R-plot of these subregions both show the similarity of the crater populations on these two terrains at $D < \sim 22$ km, implying that both of these plains units were emplaced at a similar time. The overall density of craters with $D \geq 10$ km in the exterior plains (considering these sub-regions together) is $N(10) = 60 \pm 14$, which is less than in the Caloris interior plains as shown in Fig. 8, $N(10) = 71 \pm 11$, in agreement with Strom et al. (2008). By comparison, the best estimates for the same metric for the Caloris event are $N(10) = 126 \pm 20$ from the count on the Caloris sculpture, and $N(10) = 103 \pm 16$ from the count on the Caloris rim (Fig. 8B). The latter of these two estimates is likely a minimum, given that craters having $D \sim 10$–20 km may be missing in the rim data (Fig. 8C). These results provide strong evidence that both the interior and exterior Caloris plains significantly postdate the basin itself.

this rough, mountainous terrain as a result of post-basin-formation geological processes. If this second explanation holds, the crater frequencies superposed on the Caloris sculpture may be a better representative of the basin itself in this size range.

Crater counting also provides insight into the nature and origin of the Odin Formation. As described above, the Odin Formation is characterized by terrain with dense regions of kilometer-scale knobs, surrounded and interspersed by smooth, knob-free regions (Fig. 5). One possibility is that these regions of smoother plains are younger than, and embay, the knobby terrain. If this interpretation is correct, we might expect that the smoother parts of the circum-Caloris plains have fewer superposed craters than the knobby portions. To test this idea, we measured the crater-size frequency distribution in areas with predominantly smooth plains and compared these with regions having a knobby surface texture (Fig. 9). In these two regions, we find no statistically significant difference between the crater densities at diameters 2.8 to 22 km. Moreover, the crater distributions on both the knobby Odin Formation and other, smoother portions of the plains imply that they were resurfaced after the Caloris event (compare Fig. 8C and F). This resurfacing must have been sufficient to bury craters in this 2.8–22-km-diameter range. Such burial would be consistent with the plains having a typical thickness of at least ~2 km, on the basis of fresh crater geometries (Pike, 1988). From our data, the best estimate for the density of craters on these smooth plains is $N(10) = 61 \pm 17$.

For craters at larger diameters ($D > 20$ km), the knobby Odin Formation does appear to have a higher crater frequency than the smooth plains, albeit with poor counting statistics; the seven craters with $D \geq 20$ km in the knobby facies would imply an $N(20) = 37 \pm 13$, still younger than the basin itself at high confidence. The preservation of these larger craters is consistent with a scenario under which the knobby terrain has been buried or embayed by smooth plains, which may be thinnest in regions where we can still perceive the knobby texture of the underlying terrain and remnants of the population of large, pre-plains craters. In these knobbier regions, plains emplacement may thus have been insufficient to fully bury or obscure the knobby texture and all pre-existing craters with $D > 20$ km, in contrast to the smoother regions, where the knobby texture was buried completely and the crater population more fully reset. If this is the case, the characteristic knobby texture of the Odin Formation may be inherited from the Caloris-forming event, even if it has been resurfaced in broad regions and commonly buried to significant depth.

It is worth noting that our new observations of the crater-size frequency distribution for the Caloris event and surrounding plains are consistent with some Mariner 10 estimates. Spudis and Guest (1988) quote a reference crater density for Caloris of $N(20) = 58 \pm 13$ and $N(20) = 4 \pm 7$ for Caloris exterior plains, which are both consistent with our data; if we aggregate the two subregions of exterior plains in Fig. 8D–F, for instance, we find $N(20) = 25 \pm 9$. However, many Mariner 10 estimates of the crater population for the Caloris basin have fewer craters [$N(20)$ ~20–40 and $N(10)$ ~60–80] than our estimates (Strom and Neukum, 1988; Neukum et al., 2001). These counts also show minimal differences between the basin and the interior or exterior plains (Strom and Neukum, 1988; Neukum et al., 2001); indeed, some workers have relied on the Odin Formation or interior plains to estimate an age for the basin itself. Our new data clearly show a large contrast in crater densities between the basin and the plains (Fig. 8B), so the geological relationship between the basin, the Odin Formation, and other plains warrant re-evaluation (see Section 4.4 for further discussion).

4. Discussion

4.1. The morphometry of Caloris

We have determined a best-fit ellipse for the rim of Caloris by fitting the locations of Caloris Montes material in MESSENGER and Mariner 10 data (excluding the north rim where uncertainty in the location exists) (Fig. 5A). We find an ellipse whose major axis is inclined 10° counter-clockwise from east–west, with a semi-major axis, a, of length 1525 km and a semi-minor axis, b, of length 1315 km. This basin is larger than was inferred on the basis of Mariner 10 alone (circular with D ~ 1340 km) but smaller than the initial measurements incorporating the new MESSENGER data (D ~ 1550 km). It is worth noting that such an ellipse is consistent with mapping of the main rim on the basis of Mariner 10 data alone (e.g., Spudis and Guest, 1988), because the long axis of the ellipse we infer was not fully observed during the Mariner 10 flybys. We hypothesize that this long axis may represent the direction of impact.

The best-fit ellipse we determined implies an ellipticity ratio of semimajor axis to semiminor axis $a/b = 1.16$ for Caloris, which is comparable to, or somewhat less than, many other large basins in the Solar System (Hellas Basin on Mars, $a/b = 2414/1820 = 1.33$; South-Pole Aitken, $a/b = 2125/1542 = 1.38$; Andrews-Hanna et al., 2008). We have used this same ellipse-fitting routine to find the best-fit ellipse for the Imbrium basin, which yielded a best-fit ellipse with a semi-major axis of 1165 km (essentially equal to the value given by Spudis, 1993), a semi-minor axis of 1077 km, and an ellipticity ratio $a/b = 1.08$.

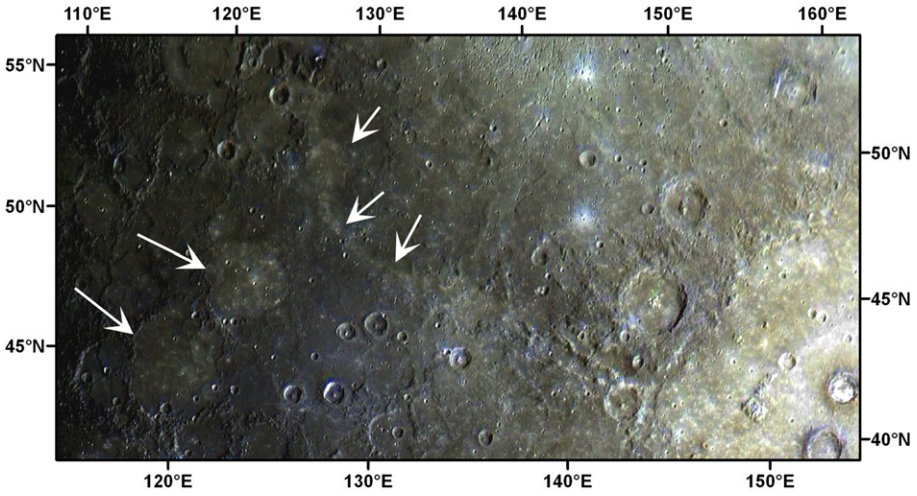

Fig. 9. Color composite of the region northwest of the Caloris basin. Data from the 480-nm, 750-nm, and 1000-nm bands of the MDIS WAC departure color sequence were assigned to blue, green, and red, and merged with MDIS NAC mosaic 2 to show detail. White arrows highlight the higher-albedo smooth plains, which appear to embay surrounding units such as the Odin Formation.

One reason for the ellipticity of these large basins is that the curvature of the planet becomes more important to crater excavation as craters reach a significant fraction of the impacted planet's size (Marinova et al., 2008). Thus, impact angles of up to 60° from horizontal may result in elliptical craters (Marinova et al., 2008). Such impact angles can be much larger than what is required to form a non-circular crater for a smaller impact (less than about 10–15°; Melosh, 1989). Given that a greater range of impact angles can result in a non-circular crater for large basins, non-circular basins are more likely to form than smaller non-circular craters. For comparison, Caloris, Imbrium, and Hellas all have semi-major axis lengths equal to ~60–70% of their respective planetary radius, a size that may lead to a somewhat elliptical form without a highly oblique impact. Moreover, other possible effects may enhance the ellipticity of larger basins, such as differential collapse during the modification stage following impact (e.g., Head, 1974a).

The plains that comprise the floor of Caloris extend north of the best-fit ellipse for the Caloris rim (Fig. 5A). We mapped the northern contact of this plains material in detail and find that it has a broadly arcuate shape that is hard to fit as a segment of the main basin rim. Indeed, if this northern contact defines the boundary of the basin, it cannot be fit well by any ellipse (it would be best described as "egg-shaped," more elongated to the north than the south). The fact that there is no circle or ellipse that can easily incorporate the boundary of the interior plains to the north with the Caloris Montes elsewhere around the basin raises the question of why the plains extend beyond the edge of what we interpret to be the Caloris topographic rim. A plausible explanation for this geometry is that the northern sector of the basin is its most substantially buried area, analogous to the western sector of Imbrium on the Moon. One mechanism for enhancing the thickness and areal extent of plains in this region would be if it were a region of lower pre-plains topography, a suggestion that will be testable during MESSENGER's orbital phase.

4.2. New observations of the proposed Caloris ring structure

MESSENGER data support the interpretation that the main topographic rim of Caloris is equivalent to the Apennine ring of the lunar Imbrium basin, on the basis of its topographic expression, morphology, and stratigraphic relationship with Caloris Group materials (Strom et al., 1975). As is the case with Imbrium, this rim position is well beyond the location of the transient cavity. In addition to this main rim, Spudis and Guest (1988) made measurements of five other possible subdued basin rings around Caloris, which they interpreted as expressed primarily through their effect on younger surface structures. These other rings were suggested to have diameters equal to 630, 900, 2050, 2700, and 3700 km; all but the 900-km-diameter ring were considered tentative. Because the best-fit center location of Caloris has been shifted by the new MESSENGER data, some differences in the ring diameters that are measured are to be expected. Moreover, the slightly elliptical nature of Caloris makes ring determination even less easily characterized by a single number. Notwithstanding these issues, we have examined the other rings suggested by Spudis and Guest (1988), and we offer the following comments: (1) The hypothesized basin interior rings (mapped originally with diameters of 630 and 900 km on the basis of the locations of deformational features in the Caloris basin fill) are broadly consistent with structures seen in the MESSENGER data (with slightly larger diameters of ~700 km and ~1000 km, respectively). However, as these rings are represented only in post-plains structure, their connection to the original impact basin morphology in the subsurface is at best indirect. (2) The next ring at approximately ~2050 km diameter may also be recognizable in MESSENGER data (best-fit diameter in the new data is ~2020 km). Along some segments of this potential ring are observed small outcrops of lineated Van Eyck Formation, which may mark the locations of pre-Calorian material uplifted by ring formation. Similar outcrops at this radial distance appear in Mariner 10 data as well.

There is, as yet, no evidence for further basin rings at distances greater than 1250 km from the center of Caloris (i.e., ring diameters greater than 2500 km) in the MESSENGER data. It is possible that, north-to-northwest of the basin, a ring might be defined by the contact of the continuous smooth plains and rougher highlands, which is broadly concentric to Caloris over a distance of at least 1000 km. However, if this ring exists, it is approximately 1550 km from the center of the basin, which would define a ring of 3100 km diameter, nearly intermediate between the ring diameters proposed on the basis of Mariner 10 observations. Verifying the existence and further describing rings will greatly benefit from measurement of the topography of the surface by the Mercury Laser Altimeter (MLA) (Cavanaugh et al., 2007) and through high-resolution imaging, given the variety of illumination conditions expected when MESSENGER reaches mapping orbit.

4.3. The distribution of Caloris sculpture and possible implications for the Caloris event

The distribution of Caloris sculpture shown in Fig. 6 is a combination of three factors: the original emplacement of sculpture, as a direct result of the impact event; the later burial or resurfacing of Van Eyck lineated terrain after the impact; and the lighting geometry, which challenges landform recognition in currently available images of areas to the north and south of the Caloris basin. If the first of these factors exerts a strong control on the distribution, it may be possible to infer aspects of the geometry of the impact event. For the Moon, it has been suggested that the largest grooves in the Imbrium sculpture trace back to a different source point than some of the smaller sculpture (Schultz, 2001). This deduction is consistent with the interpretation that the Imbrium impact was an oblique event [~30° from horizontal, impactor traveling northwest to southeast (Schultz, 1995)], as well as with the most prominently expressed Imbrium sculpture to the southeast of the basin (Schultz, 1995).

The Caloris sculpture was traced back to its possible point of origin along great circles (by extending the lineations as straight lines in a gnomic projection). These segments provide a cluster of intersections near the basin center (Fig. 6). This cluster is consistent with the moderately elliptical shape of the basin. The peak intersection density is within ~40 km (and slightly offset to the north–northeast) of the ellipse center.

The spatial distribution of Caloris sculpture is more uniform than that of the Imbrium sculpture, and there are no obvious differences between the source point of the largest Van Eyck grooves (e.g., Fig. 7B) and smaller, more distal lineations (e.g., Fig. 7E). On both the basis of the shape of the basin (Fig. 4) and the distribution of the Caloris sculpture, the impactor that formed Caloris likely struck at only a moderately oblique impact angle, perhaps along one of the two impact azimuths coincident with the major axis of the best-fitting ellipse to the basin (10° counter-clockwise from east–west, Fig. 4).

Although the impact angle and direction can be important factors in the distribution of basin ejecta (e.g., Schultz, 1995), an additional important control on the observed distribution of textured materials is burial by subsequent events. On Mercury, the walls of furrows are sometimes observed despite burial of the trough floor, usually by plains material. This sort of burial appears to be the dominant control on where Van Eyck textures are exposed. For example, in much of the circum-Caloris smooth plains, as well as in the Odin Formation, radial texturing is entirely absent. In these regions, post-Van Eyck surficial deposits are potentially thick (up to a few kilometers). However, many of the plains are probably less than 1–2 km deep, as in some locations radial texture remains visible even in otherwise typical plains (Fig. 7F).

4.4. The Odin Formation and other circum-Caloris plains: volcanic deposits, not impact ejecta

The relationship of the circum-Caloris plains to the basin itself is a long-standing question that MESSENGER data can address from a

variety of perspectives (e.g. Strom et al., 2008; Murchie et al., 2008; Robinson et al., 2008). There are two main hypotheses for the general origin of these plains, which were first observed around the eastern portion of Caloris in Mariner 10 images and now can be extended to the west of the basin with MESSENGER data: volcanic emplacement (e.g., Murray et al., 1974; Strom et al., 1975; Trask and Strom, 1976) and impact-related ejecta deposition and sedimentation (Wilhelms, 1976a).

In some regions, stratigraphic relationships alone in MESSENGER data imply that the exterior plains are unrelated to the basin. For example, northwest of Caloris (Fig. 9), some areas of plains have distinctly higher reflectance than the plains that surround them (Fig. 9; white arrows). The distribution of these higher-reflectance plains appears to be controlled by local topography, as the primary locations are in large impact craters and in a region co-aligned with, and perhaps controlled by, a large Van Eyck lineation trough. Given the coherency of these high-reflectance plains materials, and relationships suggesting that they embay surrounding plains, these materials are likely volcanic in origin (see also Murchie et al., 2008; Head et al., 2008, 2009-this issue).

In contrast, there are broad regions of the exterior plains whose stratigraphic relationship with the Caloris basin and other plains units is not as clear. The knobby texture of the Odin Formation is similar to that of the Alpes Formation interpreted as an ejecta facies associated with the Imbrium basin (McCauley et al., 1981). Other lunar basins such as Nectaris (Spudis et al., 1989) and Orientale (McCauley et al., 1981) have similar facies on their interior, or in their immediate exterior, as does the younger, multi-ring basin Raditladi ($D = 250$ km; Prockter et al., 2009) on Mercury. Formation of these knobs during impact may be a result of slumping and deformation of large ejecta blocks during the modification stage of the impact, similar to what has been suggested for the Montes Rook Formation inside Orientale (Head, 1974b). However, the detailed modes of formation that led to the observed geomorphology of the knobby plains in the Odin Formation, and in equivalent lunar facies, require further analysis.

The primary argument that the Odin Formation was not emplaced as ejecta from Caloris comes from the crater size-frequency data discussed in Section 3. Both our crater counts (Fig. 8) as well as more regional crater counts by Strom et al. (2008) on these plains units imply that they are similar in age, or younger than, the interior plains of Caloris. In turn, both the interior plains and these exterior plains have a significantly lower crater density than that inferred for the basin itself (Fig. 8). This difference indicates that the present surface of the Odin Formation and other plains materials surrounding Caloris are not ejecta deposits. Rather the region must have experienced widespread volcanic resurfacing to a depth sufficient to bury craters having diameters less than 20 km in size over a broad region.

Units on Mercury similar in geomorphic setting to lunar light plains such as the Cayley Formation are candidates for being emplaced by ballistic sedimentation during the Caloris-forming event. The best candidate regions are plains in the cratered highlands, adjacent to areas of dense Van Eyck lineations (e.g., Fig. 7D,E). Measurements on even these plains units, however, suggest they have crater size-frequency distributions similar to other exterior smooth plains deposits and thus fewer craters than would be expected if they were associated with the Caloris event itself. This result supports the view that the plains adjacent to the Van Eyck lineations are also volcanic in origin.

It is worth noting that a deficit of craters has been documented in some lunar light plains thought to be associated with particular basin-forming events (see discussion, Wilhelms, 1987, pp. 215–216; see also Boyce et al., 1974; Neukum, 1977). The reasons for this deficit are unclear. If the link between these plains units and particular basin-forming impacts is correct, it is possible that some characteristic of ballistically emplaced plains may render them susceptible to having their crater size-frequency distributions reset by later events (Boyce et al., 1974) or to their forming smaller craters than would normally be expected. Further work is necessary to understand the crater size-frequency distribution of these types of plains units on both the Moon and Mercury.

In summary, measurements of crater size-frequency distribution by several groups are inconsistent with an origin for the circum-Caloris plains by ejecta deposition, notwithstanding that morphological and color evidence are consistent with such a formation mechanism. Given this result, the origin of the knobby texture of the Odin Formation is uncertain. It is possible that the knobs are Caloris ejecta blocks that have been mostly embayed and buried by younger volcanic deposits. This is the hypothesis we presently favor. Alternatively, the knobs may be small volcanic constructs, perhaps directly connected to the emplacement of the circum-Caloris plains. The higher-resolution images at improved coverage and under a variety of illumination conditions, as well as topographic and spectral reflectance measurements, that will be obtained during MESSENGER's orbital mission phase should allow these hypotheses to be tested more fully and will sharpen the definition of the crater size-frequency distributions on these units and the Caloris basin itself.

5. Conclusions

MESSENGER image data have provided a much more complete picture of the Caloris basin and its surroundings than was available from Mariner 10. From these new observations we have evaluated the stratigraphy derived from Mariner 10 data and derived a new understanding of the basin and its surroundings. We find that:

(1) The Caloris Group, as defined on the basis of Mariner 10 data, is broadly supported by MESSENGER data, with the Caloris Montes, Odin Formation, and Van Eyck Formation clearly recognizable in the new images. The Nervo Formation (thought to be impact melt or fallback ejecta), however, is not clearly recognizable in the new data.

(2) The Caloris basin is ~15% larger than estimated on the basis of Mariner 10 images, and it has a somewhat elliptical planform (estimated ellipticity ratio $a/b = 1.16$). A comparison of this ellipticity with those of large basins on other terrestrial planets suggests that this outcome is not unusual and does not require a highly oblique impact. The impactor may have traveled along a direction of impact aligned with the major axis of the best-fit ellipse, approximately east–west (Fig. 5).

(3) Caloris sculpture can be traced over much of the Mercury surface, as can secondary craters associated with the basin, although definitively establishing which individual secondary craters or clusters are linked to Caloris is difficult.

(4) The Caloris basin itself is resolvably older than its surrounding plains, indicating that the circum-Caloris plains are not a direct result of basin formation. These plains thus are likely predominantly volcanic in origin. The knobs in the Odin formation may have originally been emplaced as ejecta and then buried and embayed by younger volcanic deposits, or they may have been formed by some other process.

(5) Further interpretation of the exterior stratigraphy of the Caloris basin will be aided by MESSENGER high-resolution color image, spectrometer, altimeter, and gravity anomaly data that will be acquired during the mission orbital phase.

Acknowledgments

We thank two anonymous reviewers, whose suggestions substantially improved this contribution. We also acknowledge Debra Hurwitz, Laura Kerber, Joe Levy, Gareth Morgan, and Sam Schon for their helpful discussions. The MESSENGER Project is supported by the NASA Discovery Program through contracts NASW-00002 with the Carnegie Institution of Washington and NAS5-97271 with the Johns Hopkins University Applied Physics Laboratory.

References

Andrews-Hanna, J.C., Zuber, M.T., Banerdt, W.B., 2008. The Borealis basin and the origin of the martian crustal dichotomy. Nature 453, 1212–1215.

Baldwin, R.B., 1963. The Measure of the Moon. University of Chicago Press, Chicago, Ill. 488 pp.

Boyce, J.M., Dial, A.L., Soderblom, L.A., 1974. Ages of the lunar nearside light plains and maria. Proc. Lunar Sci. Conf. 5, 11–23.

Cavanaugh, J.F., Smith, J.C., Sun, X., Bartels, A.E., Ramos-Izquierdo, L., Krebs, D.J., McGarry, J.F., Trunzo, R., Novo-Gradac, A.M., Britt, J.L., Karsh, J., Katz, R.B., Lukemire, A.T., Szymkiewicz, R., Berry, D.L., Swinski, J.P., Neumann, G.A., Zuber, M.T., Smith, D.E., 2007. The Mercury Laser Altimeter instrument on the MESSENGER mission. Space Sci. Rev. 131, 451–479.

Fassett, C.I., Head, J.W., 2008. The timing of martian valley network activity: constraints from buffered crater counting. Icarus 195, 61–89.

Gilbert, G.K., 1893. The Moon's face: a study of the origin of its features. Bull. Phil. Soc. Wash. 12, 241–292.

Guest, J.E., Greeley, R., 1983. Geologic map of the Shakespeare quadrangle of Mercury (H-3). Map I-1408, Misc. Investigations Ser., U. S. Geological Survey, Denver, Colo.

Hartmann, W.K., 1963. Radial structures surrounding lunar basins: I. The Imbrium system. Commun. Lunar Planet. Lab. 2, 1–15.

Haskin, L.A., 1998. The Imbrium impact event and the thorium distribution at the lunar highlands surface. J. Geophys. Res. 103, 1679–1689.

Haskin, L.A., Korotev, R.L., Rockow, K.M., Jolliff, B.L., 1998. The case for an Imbrium origin of the Apollo thorium-rich impact-melt breccias. Meteorit. Planet. Sci. 33, 959–975.

Hawkins III, S.E., Boldt, J.D., Darlington, E.H., Espiritu, R., Gold, R.E., Gotwols, B., Grey, M.P., Hash, C.D., Hayes, J.R., Jaskulek, S.E., Kardian, C.J., Keller, M.R., Malaret, E.R., Murchie, S.L., Murphy, P.K., Peacock, K., Prockter, L.M., Reiter, R.A., Robinson, M.S., Schaefer, E.D., Shelton, R.G., Sterner II, R.E., Taylor, H.W., Watters, T.R., Williams, B.D., 2007. The Mercury Dual Imaging System on the MESSENGER spacecraft. Space Sci. Rev. 131, 247–338.

Head, J.W., 1974a. Orientale multi-ringed basin interior and implications for petrogenesis of the lunar samples. Moon 11, 327–356.

Head, J.W., 1974b. Stratigraphy of the Descartes region (Apollo 16): implications for the origin of samples. Moon 11, 77–99.

Head, J.W., 1975. Processes of lunar crater degradation: changes in style with geologic time. Moon 12, 299–329.

Head, J.W., Murchie, S.L., Prockter, L.M., Robinson, M.S., Solomon, S.C., Strom, R.G., Chapman, C.R., Watters, T.R., McClintock, W.E., Blewett, D.T., Gillis-Davis, J.J., 2008. Volcanism on Mercury: evidence from the first MESSENGER flyby. Science 321, 69–72.

Head, J.W., Murchie, S.L., Prockter, L.M., Solomon, S.C., Chapman, C.R., Strom, R.G., Watters, T.R., Blewett, D.T., Gillis-Davis, J.J., Fassett, C.I., Dickson, J.L., Morgan, G.A., Kerber, L., 2009. Volcanism on Mercury: Evidence from the first MESSENGER flyby for extrusive and explosive activity and the volcanic origin of plains. Earth Planet. Sci. Lett., 285, 227–242 (this issue).

Marinova, M.M., Aharonson, O., Asphaug, E., 2008. Mega-impact formation of the Mars hemispheric dichotomy. Nature 453, 1216–1219.

McCauley, J.F., 1977. Orientale and Caloris. Phys. Earth Planet. Inter. 15, 220–250.

McCauley, J.F., Guest, J.E., Schaber, G.G., Trask, N.J., Greeley, R., 1981. Stratigraphy of the Caloris basin, Mercury. Icarus 47, 184–202.

McGetchin, T.R., Settle, M., Head, J.W., 1973. Radial thickness variation in impact crater ejecta: implications for lunar basin deposits. Earth Planet. Sci. Lett. 20, 226–236.

Melosh, H.J., 1989. Impact Cratering: A Geologic Process. Oxford University Press, New York. 245 pp.

Murchie, S.L., Watters, T.R., Robinson, M.S., Head, J.W., Strom, R.G., Chapman, C.R., Solomon, S.C., McClintock, W.E., Prockter, L.M., Domingue, D.L., Blewett, D.T., 2008. Geology of the Caloris basin, Mercury: a view from MESSENGER. Science 321, 73–76.

Murray, B.C., Belton, M.J.S., Danielson, G.E., Davies, M.E., Gault, D.E., Hapke, B., O'Leary, B., Strom, R.G., Suomi, V., Trask, N., 1974. Mercury's surface: preliminary description and interpretation from Mariner 10 pictures. Science 185, 169–179.

Neukum, G., 1977. Different ages of lunar light plains. Moon 17, 383–393.

Neukum, G., Oberst, J., Hoffmann, H., Wagner, R., Ivanov, B.A., 2001. Geologic evolution and cratering history of Mercury. Planet. Space Sci. 49, 1507–1521.

Oberbeck, V.R., 1975. The role of ballistic erosion and sedimentation in lunar stratigraphy. Rev. Geophys. Space Phys. 13, 337–362.

Oberbeck, V.R., Hörz, F., Morrison, R.H., Quaide, W.L., Gault, D.E., 1975. On the origin of lunar smooth plains. Moon 12, 19–54.

Petro, N.E., Pieters, C.M., 2005. Lunar-wide effects of basin formation on the lunar crust. Lunar Planet. Sci. 36, abstract 1209.

Petro, N.E., Pieters, C.M., 2006. Modeling the provenance of the Apollo 16 regolith. J. Geophys. Res. 111, E09005. doi:10.1029/2005JE002559.

Pike, R.J., 1988. Geomorphology of impact craters on Mercury. In: Vilas, F., Chapman, C.R., Matthews, M.S. (Eds.), Mercury. University of Arizona Press, Tucson, Ariz., pp. 165–273.

Prockter, L.M., Watters, T.R., Chapman, C.R., Denevi, B.W., Head, J.W., Solomon, S.C., Murchie, S.L., Barnouin-Jha, O.S., Robinson, M.S., Blewett, D.T., Gillis-Davis, J., Gaskell, R.W., 2009. The curious case of Raditladi basin. Lunar Planet. Sci. 40, abstract 1758.

Robinson, M.S., Murchie, S.L., Blewett, D.T., Domingue, D.L., Hawkins, S.E., Head, J.W., Holsclaw, G.M., McClintock, W.E., McCoy, T.J., McNutt, R.L., Prockter, L.M., Solomon, S.C., Watters, T.R., 2008. Reflectance and color variations on Mercury: indicators of regolith processes and compositional heterogeneity. Science 321, 66–69.

Schaber, G.G., McCauley, J.F., 1980. Geologic map of the Tolstoj quadrangle of Mercury (H-8). Map I-1199, Misc. Investigations Ser., U. S. Geological Survey, Denver, Colo.

Schultz, P.H., 1995. Making the man in the Moon: origin of the Imbrium basin. Lunar Planet. Sci. 16, 1251–1252.

Schultz, P.H., 2001. Origin and implications of the Imbrium sculpture. Lunar Planet. Sci. 32, abstract 1900.

Shoemaker, E.M., Hackman, R.J., 1962. Stratigraphic basis for a lunar time scale. In: Kopal, Z., Mikhailov, Z.K. (Eds.), The Moon. Academic Press, New York, pp. 289–300.

Solomon, S.C., McNutt, R.L., Watters, T.R., Lawrence, D.J., Feldman, W.C., Head, J.W., Krimigis, S.M., Murchie, S.L., Phillips, R.J., Slavin, J.A., Zuber, M.T., 2008. Return to Mercury: a global perspective on MESSENGER's first Mercury flyby. Science 321, 59–62.

Spudis, P.D., 1984. Apollo 16 site geology and impact melts: implications for the geologic history of the lunar highlands. Proc. Lunar Planet. Sci. Conf. 15, C95–C107.

Spudis, P.D., 1993. The Geology of Multi-Ring Impact Basins. Cambridge University Press, Cambridge, UK. 263 pp.

Spudis, P.D., Guest, J.E., 1988. Stratigraphy and geologic history of Mercury. In: Vilas, F., Chapman, C.R., Matthews, M.S. (Eds.), Mercury. University of Arizona Press, Tucson, Ariz., pp. 118–164.

Spudis, P.D., Hawke, B.R., Lucey, P.G., 1989. Geology and deposits of the lunar Nectaris basin. Proc. Lunar Planet. Sci. Conf. 19, 51–59.

Stöffler, D., Bischoff, A., Borchardt, R., Burghele, A., Deutsch, A., Jessberger, E.K., Ostertag, R., Palme, H., Spettel, B., Reimold, W.U., Wacker, K., Wanke, H., 1985. Composition and evolution of the lunar crust in the Descartes Highlands, Apollo 16. Proc. Lunar Planet. Sci. Conf. 15, C449–C506.

Strom, R.G., Neukum, G., 1988. The cratering record on Mercury and the origin of impacting objects. In: Vilas, F., Chapman, C.R., Matthews, M.S. (Eds.), Mercury. University of Arizona Press, Tucson, Ariz., pp. 336–373.

Strom, R.G., Trask, N.J., Guest, J.E., 1975. Tectonism and volcanism on Mercury. J. Geophys. Res. 80, 2478–2507.

Strom, R.G., Malhotra, R., Ito, T., Yoshida, F., Kring, D.A., 2005. The origin of planetary impactors in the inner solar system. Science 309, 1847–1850.

Strom, R.G., Chapman, C.R., Merline, W.J., Solomon, S.C., Head, J.W., 2008. Mercury cratering record viewed from MESSENGER's first flyby. Science 321, 79–81.

Tanaka, K.L., 1982. A new time-saving crater-count technique with application to narrow features. Reports of Planetary Geology — 1982. NASA Tech. Memo., TM-85127, pp. 123–125.

Trask, N.J., Strom, R.G., 1976. Additional evidence of mercurian volcanism. Icarus 28, 559–563.

Watters, T.R., Murchie, S.L., Robinson, M.S., Solomon, S.C., Denevi, B.W., André, S.L., Head, L.W., 2009. Emplacement and tectonic deformation of smooth plains in the Caloris basin, Mercury. Earth Planet. Sci. Lett., 285, 309–319 (this issue).

Wilhelms, D.E., 1976a. Mercurian volcanism questioned. Icarus 28, 551–558.

Wilhelms, D.E., 1976b. Secondary impact craters of lunar basins. Proc. Lunar Sci. Conf. 7, 2883–2901.

Wilhelms, D.E., 1987. The geologic history of the Moon. Prof. Paper 1348, U. S. Geological Survey, Denver, Colo. 302 pp.